一种新型 Cu 基自蔓延焊接接头组织和性能

胡军志， 马世宁， 陈学荣， 罗 林
（装甲兵工程学院 装备再制造技术国防科技重点实验室，北京 100072）

胡军志

摘 要：针对在野外条件下金属零部件的焊接应急修理困难的问题，以 CuO＋Al 系铝热剂反应为放热源，开发了一种新型 Cu 基自蔓延焊接材料，对其焊缝的组织形貌及性能进行了研究。结果表明，自蔓延反应后形成熔焊焊接，焊缝成形良好，焊缝与基体之间存在明显的过渡区，焊缝的抗拉强度大于 200 MPa，抗弯强度接近 600 MPa，表面硬度可达 HRB130，能够满足金属零部件野外应急维修需要。

关键词：自蔓延焊接；材料；组织；性能
中图分类号：TH17，TG456.9 文献标识码：A 文章编号：0253－360X(2006)10－094－03

0 序 言

SHS，自蔓延高温合成（self-propagating high temperature synthesis）的简称，是指放热体系被点燃，形成燃烧波，利用自身放热维持反应进行，同时合成材料的工艺过程，它与传统焊接技术相结合形成了自蔓延焊接技术[1~4]。自蔓延焊接技术具有以下特点：(1)可焊接异型材料；(2)节约能源；(3)可保护母材的性能等[5]。

在野外应急以及高空、地下等无法供应能源的条件下，传统的焊接技术由于其设备、工艺、工效等原因已无法快速、有效地施展。因此开发一种具有高效、节能的新型焊接技术和材料，以弥补传统焊接技术的不足已显得非常必要。针对这一情况，以铝热剂反应为基础，即以 CuO＋Al 系铝热剂反应为放热源（理论燃烧温度为 5 151K），开发了一种新型的 Cu 基自蔓延焊接材料。其最大的特点是，焊接时只需用火柴点燃用该种焊接材料特制的焊接笔的引信即可进行，不需要其它设备和材料。作者对其焊缝的组织形貌及性能进行研究，以考察该种材料的应用可行性，为以后该材料的应用提供理论依据。

1 试验材料及试验方法

1.1 试验材料

焊接材料为研制的 Cu 基自蔓延焊接材料，制成手持式专用笔，该材料成分见表 1。被焊材料为 4 mm 厚的 45，Q235 钢板，采用对焊形式进行焊接。焊接工艺参数见表 2。以焊条电弧焊的手法进行焊接，图 1 为焊接后焊缝的形状，由图可见，焊缝成形良好。

表 1 Cu 基自蔓延焊接材料成分（质量分数，%）
Table 1 Chemical compositions of cuprum-base SHS welding material

Mg	Fe	Si	Ca
0.1~0.3	6.0~9.0	6.5~9.5	2.5~3.5
Cr	S	O	Cu
0.5~1.0	≤0.03	8.5~14.5	余量

表 2 焊接工艺参数
Table 2 technical parameters of SHS welding

焊接速度 v/(mm·s^{-1})	焊接角度 θ(°)	焊接距离 d/mm
5~7	5~10	2~4

注：点火方式为火柴点火

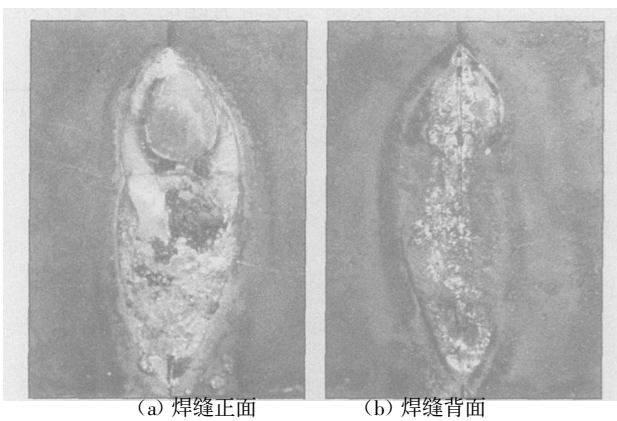

(a) 焊缝正面 (b) 焊缝背面

图 1 焊缝表面形貌
Fig. 1 Surface topography of weld

1.2 试验方法

用 OLYMPUS PMG3 金相显微镜和带有 EDAX 的

收稿日期：2005－10－10

Philips XL30 型扫描电子显微镜(SEM)分析焊缝的组织形貌；用布鲁克 D8－ADVANCED X 衍射分析仪进行焊缝 XRD 物相分析；参照国家标准 GB2651－89 和 GB2653－89 在 WA－10 万能试验机上进行焊接接头的拉伸和四点弯曲试验，试验时每种焊接接头测五个值，取平均值作为其结果。在 HBRVU－187.5 型布洛维光学硬度计上进行硬度试验，试验时以焊缝中间为起点，间隔 5 mm 进行测量。

2　结果及分析

2.1　组织形貌

图 2 为焊缝与基体的组织形貌图。从图中可以看出，基体（A 区）与焊缝（C 区）之间存在着明显的过渡区（B 区），这主要是焊接时焊接笔通过自蔓延放热反应放出大量的热量，使基材熔化，形成冶金结合；冷却后，在焊缝与基体之间形成了明显的过渡区。对焊缝中元素的线扫描可以发现，Fe 元素的含量从基体（A 区）到焊缝（C 区）逐渐减少，而 Cu 元素的含量则从基体(A 区)到焊缝(C 区)逐渐增大，而在 B 区 Fe 和 Cu 的成分连续过渡，这说明焊接时 Fe 元素和 Cu 元素在过渡区内进行了相互扩散，该过渡区就是焊接熔合区，表明该种自蔓延焊接是一种熔焊焊接。对焊缝中的各区进行能谱分析(表 3)，各元素的含量变化也证实了这一点。

表 3　焊缝中各区元素(质量分数，%)

Table 3　Chemical compositions in each area of weld

区域	Fe	Cu
A	100.00	—
B	85.95	14.05
C	2.88	97.12

图 3 为焊缝的组织形貌图。从图中可以看出，焊缝组织不均匀，这主要是由于焊缝在进行结晶的过程中冷却速度很快，金属元素来不及充分扩散，合金元素的分布出现不均匀，导致组织不均匀。整个焊缝由三种物质(A，B，C)组成。通过对这三种物质进行 EDAX 分析以及焊缝表面的 XRD 分析(图 3，图 4，表 4)，得出这些物质均由 Cu、Fe 组成；XRD 分析表明焊缝中只存在 Cu－Fe 固溶体，没有生成新相，因此这三种物质均是 Cu－Fe 固溶体，由于成分不均匀，导致形状各异。

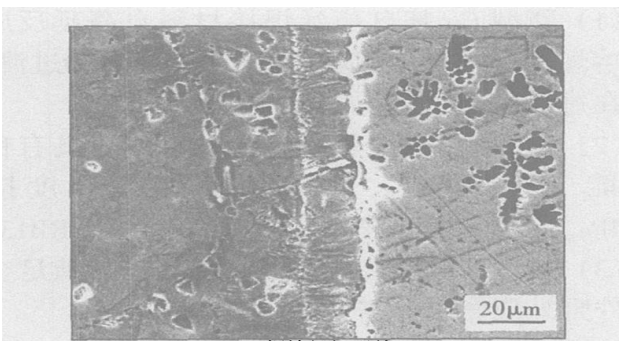

(a) 焊缝组织形貌

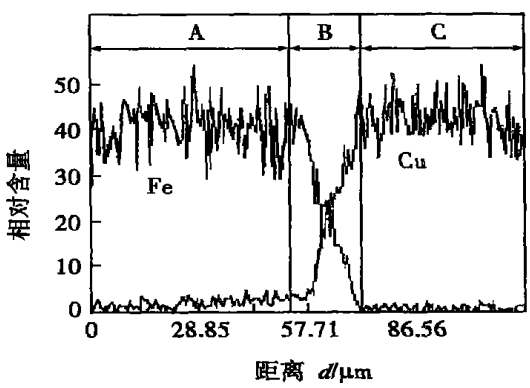

(b) 元素线扫描

图 2　Cu 基自蔓延焊接接头元素线扫描(Fe，Cu)

Fig. 2　Line scanning of Fe and Cu element for cuprum-base SHS welded joint

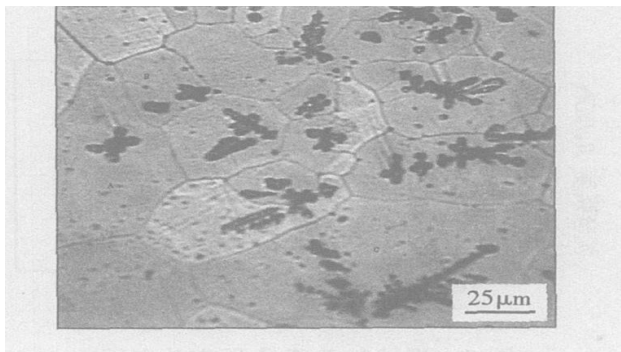

图 3　焊缝组织形貌图

Fig. 3　Structure of welding line

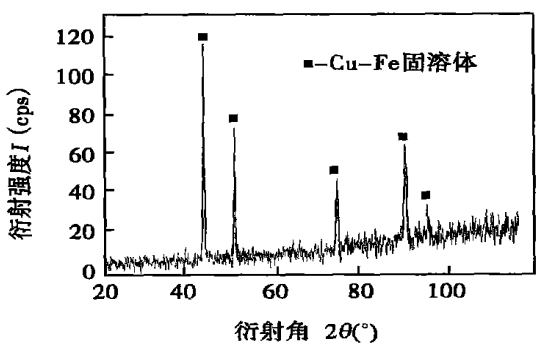

图 4　焊缝表面 X 衍射图

Fig. 4　X-ray of surface of weld

表 4 焊缝中各物质元素(质量分数,%)

Table 4 Chemical compositions of each thing in weld

区域	Fe	Cu
A	2.89	97.11
B	6.30	93.70
C	13.9	86.91

2.2 焊接接头强度

图 5,图 6 分别为焊接接头的抗拉强度和抗弯强度图。从图中可以看出,Cu 基自蔓延焊接材料焊接接头的抗拉强度超过 200 MPa,抗弯强度接近 600 MPa,均要接近 Q235 钢的强度而低于 45 钢,表明该材料焊接接头的强度较高,这是由于该种焊接是熔焊焊接,焊缝与基体以冶金结合方式进行结合。

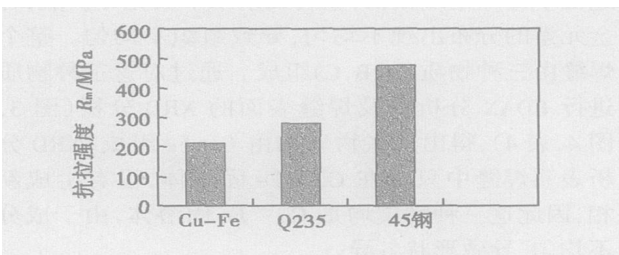

图 5 焊接接头抗拉强度分布图

Fig. 5 Bonding strength of each material

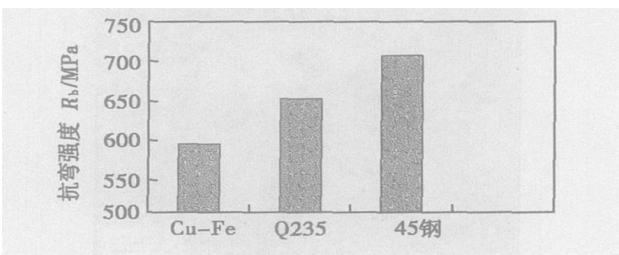

图 6 焊接接头弯曲强度分布图

Fig. 6 Bending strength of each material

2.3 焊接接头的冲击韧度

表 5 为焊接接头的冲击韧度。从表中可以看出,焊接接头的冲击韧度比较高,但要低于 Q235 钢和 45 钢,其中焊接接头正面的冲击韧度要低于反面的冲击韧度。这说明焊接时,如果进行两面焊接,焊接接头的冲击韧度可能还有一定程度的提高。

表 5 焊接接头的冲击韧度

Table 5 Impacting tenacity of welded joint

类型	弯曲方向	冲击韧度 a_{kv}/(J·cm^{-2})
Cu—Fe	正面	35.67
	反面	44.59
Q235 钢		88.20
45 钢		85.75

2.4 焊接接头与基体热影响区的硬度

图 7 为焊接接头与基体热影响区的硬度分布图。从图中可以看出,焊缝的硬度要低于热影响区的硬度。

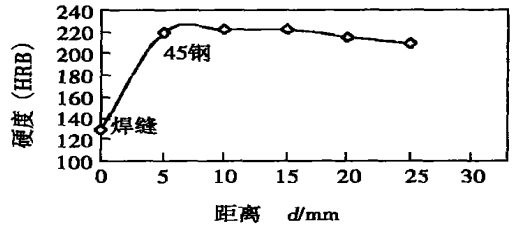

图 7 焊接接头硬度分布图

Fig. 7 Rigidity of welded joint

通过对该种 Cu 基自蔓延焊接材料的强度、冲击韧度以及表面硬度的分析测试,尽管在性能方面该材料不如 45 钢,但还是可以满足金属零部件野外应急维修需要。

3 结 论

(1) 新型 Cu 基自蔓延焊接材料自蔓延反应后形成熔焊焊接,焊缝与基体之间存在明显的过渡区,元素在过渡区进行了扩散。

(2) 新型 Cu 基自蔓延焊接材料焊缝具有良好的性能,抗拉强度大于 200 MPa,抗弯强度接近 600 MPa,抗冲击韧度较好,表面硬度可达 HRB130。

(3) 新型 Cu 基自蔓延焊接材料能够满足金属零部件野外应急维修需要。

参考文献:

[1] Merzhanov A G. Self-propagating high-temperature synthesis: twenty years of search and findings[M]. In: Combustion and Plasma Synthesis of High-temperature Materials, Ed by Munir Z A. VCH. New York: 1990

[2] Li S J. Joining of SiC Ceramics to Ni-Based Superalloy with Cu Intermediate Layer[J]. Key Engineering Materials, 2002, 27(3): 101—110

[3] 李 强,于景媛,穆柏椿. 自蔓延高温合成(SHS)技术简介[J]. 辽宁工学院学报, 2001, 21(5): 61—63

[4] 王志远. 自蔓延高温合成技术研究与应用的新进展[J]. 化工进展, 2002, 21(3): 175—178.

[5] 殷 声. 燃烧合成[M]. 北京: 冶金工业出版社, 1999.

作者简介:胡军志,男,1975 年 6 月出生,博士研究生,讲师。主要从事自蔓延焊接方面的研究。发表论文 20 余篇。

Email: hjzh1818@126.com

the maximum hoop tensile residual stress exists in the region of the start/stop point of the circular weld for above two models, where the stress distribution is complex and the larger hoop tensile stresses are always regarded as the driven force of weld fracture. As comparison, the case of the nozzle weld needs more attention.

Key words: closed weld; residual stress; finite element method; Gauss distribution; multi-pass welding; crack propagation

3-D finite element analysis of welding residual stress for half-pipe jacket made of 304 stainless steel JIANG Wen-chun, GONG Jian-ming, CHEN Hu, TU Shan-dong (Nanjing University of Technology, Nanjing 210009, China). p77—80

Abstract: The problem of half-pipe jacket equipment is the leakage induced by cracks in half-pipe welding position. Welding residual stress is one of the main influential factors. Using finite element analysis software ABAQUS, a multi-sequentially coupling finite element program was developed to calculate the welding residual stress for half-pipe jacket of 304 stainless steel. The moving Gaussian heat source was realized using the subroutine DFLUX complied by FORTRAN language. With this program and subroutine, 3-D welding residual stress field of T-joint for half-pipe was obtained and analyzed. The result shows that the stress is much larger near the T-joint zone, which induces the cracking and leakage easily sometimes. The analysis from calculation result provides theory references for optimizing the welding parameter and controlling the welding residual stress. It is of great significance for increasing the reliability and safety of half-pipe jacket equipment.

Key words: half-pipe jacket; welding residual stress; finite element method; multi-sequential coupling; ABAQUS

Mechanical properties and microstructure of TiAl/42CrMo joint induction brazed with Ag-Cu-Ni-Li filler metal LI Yu-long, HE Peng, FENG Ji-cai (State Key Laboratory of Advanced Welding Production Technology, Harbin Institute of Technology, Harbin 150001, China). p81—84

Abstract: Induction brazing of TiAl to 42CrMo steel under the protection of Ar gas was carried out with a Ag-Cu-Ni-Li filler metal. The results show that Ti_3Al, $AlCuTi$, $AlCu_2Ti$, Ag-based solid solution, Ag-Cu eutectic and TiC phase occur at the interface of the brazed joint. When the joint was brazed at 1000 ℃ for 30 s, the interface is mainly composed of the Al-Cu-Ti ternary intermetallics; its strength is not very high; crack occurs in the Al-Cu-Ti ternary intermetallics. When it was brazed at 890 ℃ for 30 s, room temperature and elevated temperature (400℃) tensile strength of the joint is up to 309 MPa and 286 MPa, respectively. Crack occurs initially at the phase boundary of the $AlCu_2Ti$ particles and the Ag-based solid solution, then expands to the reaction layers adjacent to the base metals and results in failure.

Key words: TiAl/42CrMo; induction brazing; microstructure; tensile strength

Welding arc in plasma arc welding with activated flux CHAI Guo-ming, ZHU Yi-feng (National Key Laboratory for High Energy Density Beam Processing Technology, Beijing Aeronautical Manufacturing Technology Research Instiute, Beijing 100024, China). p85—88

Abstract: The welding arc in PAW effected by activated flux was studied, and the relationship between the welding arc voltage and activated flux was also studied. In activated flux PAW, the welding arc temperature field was measured by the infrared sensing and computer image technique. The distribution models of heat flow density of welding arc in activated flux PAW were developed. The results show that the activated flux PAW arc is contractive; the arc tail is disappeared; the efflux plasma is increasing; the force of penetration is strengthened; the arc voltage is high; the welding arc temperature distribution in activated flux PAW is compact; the outline of the welding arc temperature field is narrow; the range of the welding arc temperature distribution is concentrated; the welding arc radial temperature gradient is large; the welding arc radial temperature gradient shows normal Gauss distribution. The result shows that there is little difference in mechanical properties between the welded joints with activated flux and that without activated flux.

Key words: activated flux plasma arc welding; welding arc; temperature field

Infrared measurement and numerical simulation of temperature field in hybrid laser-TIG welding process of magnesium alloys HUANG Rui-sheng, LIU Li-ming, CHI Ming-sheng (State Key Laboratory of Material Surface Modification by Laser, Ion, and Electronic beams, Dalian University of Technology, Dalian 116024, China). p89—93

Abstract: The infrared thermal imaging system was used as a sensor to measure the temperature field of wrought magnesium alloy AZ31B during the laser-TIG hybrid welding process. And a method for calibrating the welding temperature field was proposed, that was based on the infrared temperature measurement theory and was directed toward the infrared thermal imaging system. Thermocouple was applied to verify the accuracy of the calibrated method. And numerical simulation method was used to simulate the whole welding temperature field. The experiment results showed that real temperature calibrated method was able to calibrate the temperature field accurately when the plate surface condition was uniform, and surface calibrated method was able to keep the influence caused by the plate surface condition alternation from the temperature field distribution. With the combination of real temperature calibrated method and surface calibrated method, exact temperature field of magnesium alloy outside the arc covering area during laser-TIG hybrid welding process was obtained. Welding temperature field numerical simulation method was able to forecast and reflect the real distribution of whole welding temperature field accurately.

Key words: magnesium alloy; laser-TIG hybrid welding; temperature field; infrared; numerical simulation

Structure and performance of a new Cu-base SHS welded joint HU Jun-zhi, MA Shi-ning, CHEN Xue-rong, LUO Lin (Armored Force Engineering Academy, National Key Laboratory for Re-

manufacturing, Beijing 100072, China). p94—96

Abstract: A new cuprum-base SHS welding material was developed by SHS combustion between CuO and Al in order to solve a problem that welding mend of metal parts was difficult in field. The structure and performances of the welded joint were studied. The results indicated that the welding was fusion welding, and weld appearance is good. Transition zone was clear between base metal and weld metal. At the same time, tensile strength of the welded joint was higher than 200 MPa, and bending strength was close to 600 MPa and surface hardness was also close to HRB130. It also indicated this technology can meet the need of repair of metal parts in field.

Key words: SHS welding; material; structure; performance

Effect of welding thermal cycle on toughness of continuous casting steel center YAO Shang-wei[1, 2], ZHAO Lu-yu[2], XU Ke[2], WANG Ren-fu[2] (1. Department of Mechanical Engineering, Xi'an Jiao tong University, Xi'an 710049, China; 2. Luoyang Ship Materials Research Institute, Luoyang 471039, Henan, China). p97—100

Abstract: Using welding thermal simulation, the effect of welding thermal cycle on impact toughness was investigated by means of charpy impart test and metalographic test, whose specimens were samplinged from surface and center of continuous casting 10CrNi3MoV steel. The results show that center segregation deteriorates the impact toughenss of center part and the parameter of welding thermal cycle has different effect on toughenss of steel. The reasons for physical and metallurgical factor are the element segregation of C and S and the difference in structure and grain size which has subjected to different welding thermal cycle.

Key words: center segregation; welding thermal cycle; continuous casting steel; toughness

Compiling and interpreting system of hybrid arc welding robot language ZHANG Lian-xin, GAO Hong-ming, ZHANG Guang-jun, WU Lin (State Key Laboratory of Advanced Welding Production Technology, Harbin Institute of Technology, Harbin 150001, China). p101—104

Abstract: The compiling and interpreting system of hybrid arc welding robot language (HAWRL) was developed. Firstly, by analyzing the characteristics of source code and object code, the architecture of compiling and interpreting system, which includes morphology/syntax analysis, semantic analysis, error handling, symbol table manager and object code generation, was presented. Secondly, on the base of classifying key words of HAWRL, three module of the morphology/syntax analysis, semantic analysis and object code generation are developed. At last, experiment was executed to compile and interpret HAWRL programs that obtained from all kinds of methods. The results show that the compiling and interpreting system not only can compile HAWRL program to PMAC motion program correctly, but also can help user to debug and revise the source program with errors efficiently.

Key words: compiling and interpreting; robot language; architecture; arc welding robot

Comparison of 3D and 2D numerical simulation of continuous-drive friction welding process ZHANG Quan-zhong[1, 2], ZHANG Li-wen[1, 2], LIU Wei-wei[2], ZHANG Xing-guo[1, 2], QU Shen[3], ZHU Wen-hui[3] (1. State Key Laboratory of Material Surface Modification, Dalian University of Technology, Dalian 116024, China; 2. School of Materials Science and Engineering, Dalian University of Technology, Dalian 116024, China; 3. Shenyang Liming Aero-Engine Group Corporation, Shenyang 110043, China). p105—108

Abstract: The 3D and 2D rigid-plastic thermo-mechanical coupled finite element models of continuous-drive friction welding process were developed. In 3D model, the tangential frictional-force in friction interface was considered. The transient temperature field, stress field and deformation field during the continuous-drive friction welding process of GH4169 rod are calculated respectively using these two models. The results of 3D and 2D simulation were compared. Meanwhile, both of the simulation results were compared with those of experiments. It's found that there is no appreciable difference in the calculated temperature between 3D and 2D simulation, and they both have a good agreement with the experimental results. But when compared to the results of 2D simulation, the calculated equivalent stress with 3D model is higher and more reliable, and the flash shape and axial shortening fit the experimental results better. So the 3D model can more accurately predict the friction welding process.

Key words: continuous-drive friction welding; numerical simulation; 3D model; 2D axisymmetric model

Effect of welding thermal cycle on HAZ microstructure and mechanical properties of copper-bearing age-hardening steels CHAI Feng[1,2], YANG Cai-fu[2], ZHANG Yong-quan[2], HANG Su[2], XU Zhou[1] (1. Shanghai Jiaotong University, Shanghai 200030, China; 2. Central Iron and Steel Research Institute, Beijing 100081, China). p109—112

Abstract: Effect of welding thermal cycle on microstructure and mechanical properties of copper-bearing age hardening steel were studied. The results showed that there was significant difference on mechanical properties in different region of HAZ after single welding thermal cycle. Coarse-grain region has the poor impact toughness in HAZ because of growth of austenite grain and increasing amount of granular-binaite. Intercritical region is the softened region in HAZ which is due to coarsening and redissolving of precipitate phase and increasing amount of ferrite. Double thermal cycle has great impact toughress on HAZ microstructures and properties. CGHAZ+ICHAZ is region which has the worst mechanic properties after double thermal cycle because of increase of amount and size of granular bainite.

Key words: copper-bearing age-hardening steel; heat affected zone; coarse-grain region; fine-grain region; intercritical region